



CHORUS

This is the accepted manuscript made available via CHORUS. The article has been published as:

Self-Calibrating Vector Atomic Magnetometry through Microwave Polarization Reconstruction

T. Thiele, Y. Lin, M. O. Brown, and C. A. Regal

Phys. Rev. Lett. **121**, 153202 — Published 8 October 2018

DOI: [10.1103/PhysRevLett.121.153202](https://doi.org/10.1103/PhysRevLett.121.153202)

Self-calibrating vector atomic magnetometry through microwave polarization reconstruction

T. Thiele,^{1,*} Y. Lin,^{1,†} M. O. Brown,¹ and C. A. Regal¹

¹*JILA, National Institute of Standards and Technology and University of Colorado, and Department of Physics, University of Colorado, Boulder, Colorado 80309, USA*

Atomic magnetometry is one of the most sensitive ways to measure magnetic fields. We present a method for converting a naturally scalar atomic magnetometer into a vector magnetometer by exploiting the polarization dependence of hyperfine transitions in rubidium atoms. First, we fully determine the polarization ellipse of an applied microwave field using a self-calibrating method, *i.e.* a method in which the light-atom interaction provides everything required to know the field in an orthogonal laboratory frame. We then measure the direction of an applied static field using the polarization ellipse as a three-dimensional reference defined by Maxwell's equations. Although demonstrated with trapped atoms, this technique could be applied to atomic vapors, or a variety of atom-like systems.

Sensitive magnetometers are increasingly important in both fundamental and technological applications. High accuracy and precision magnetometers are used for dark matter searches and aid in tests of fundamental symmetries. They enable applications ranging from navigation, timekeeping, and geophysical measurement to biological imaging. A wide array of application-specific requirements has yielded a wide array of magnetometry technologies, drawing on atomic vapors [1, 2], nitrogen-vacancy centers [3], nuclear magnetic resonance [4], and superconducting quantum-interference devices [5].

For many magnetometry applications measurement of the scalar field is sufficient, but also knowing the field's full vector description can have important implications, in particular in geosensing [6–8] and the calibration of precision physics experiments [9]. However, mapping a magnetic field in three-dimensional space with a robust calibration is nontrivial, and presents distinct challenges in different platforms.

Superconducting quantum interference devices (SQUIDS) and Hall or fluxgate sensors are naturally sensitive to a field component perpendicular to, for example, a current loop. But multiple sensors must be used to measure the field in all three dimensions, and common problems are drifts or uncertainties in the relative directions of the axes [10, 11]. Solid-state sensors such as nitrogen vacancy (NV) centers in diamond have emerged as a robust and broadband room-temperature platform for magnetic sensing and imaging. The inherent crystalline structure of NVs provides a natural reference for vector sensing that is actively being developed [12–17].

The most precise magnetometers, which reach sensitivities beyond fT/\sqrt{Hz} , are atomic magnetometers that consist of many indistinguishable atoms in the vapor phase [18]. However, as they are based on Larmor precession, they are scalar sensors, and there is no natural knob for breaking down the total field into components. In the most standard approach to an atomic vector mag-

netometer, vector addition of an applied static bias field and the field to be measured can be used to extract the unknown field direction [19–21]. However, knowledge of the applied bias fields in a orthogonal laboratory frame is limited by the calibration of the external coil set used to apply the bias field. To avoid reliance upon mechanical construction tolerances for calibration, a number of ideas have been developed for atomic vector magnetometers, such as double-resonance magnetometers [22–24], the use of electromagnetically-induced-transparency effects [25, 26], and orthogonal pump beams and effective fields of optical light [27].

In this Letter, we introduce a spatial reference for vector atomic magnetometry based upon the three-dimensional structure of a microwave field. Our work draws on advances in microwave-field measurements and imaging using atoms [28–30]. In these techniques, a microwave field can be characterized through the atomic response the microwave radiation with respect to an applied quantization axis. In our work, we demonstrate a general algorithm for full reconstruction of a microwave polarization ellipse based upon atomic measurements. Importantly, we show self-calibration of the three-dimensional ellipse: Systematics in the direction and strength of applied bias fields, *e.g.* non-orthogonal field orientations, can be located and corrected based upon the expected atomic response and electro-magnetic field structure.

Using the reconstructed microwave polarization ellipse as a fundamental reference, we demonstrate atomic vector magnetometry. We measure the strength and direction of an applied static magnetic field using only the microwave polarization information and the strength of atomic transitions, without the need for rotation of additional static fields. Our magnetometer can operate in either small field or with an applied reference field.

Our experiments take place using single trapped alkali atoms; while the sensitivity of the experiment undertaken with a few atoms is limited, it enables a proof-of-principle

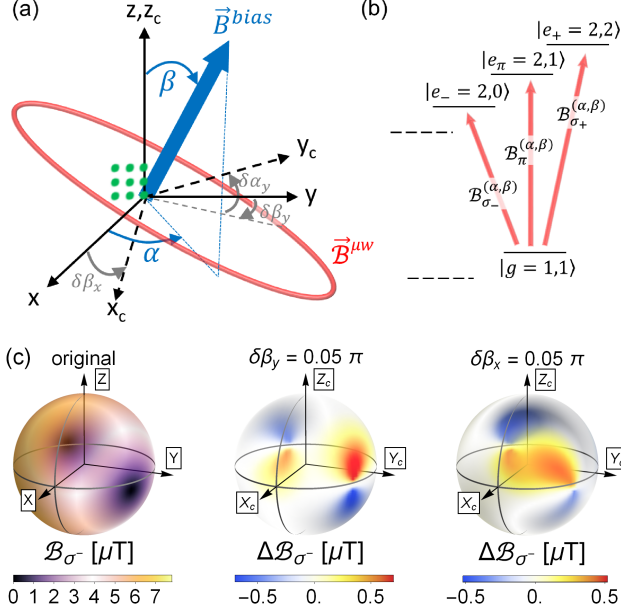


FIG. 1. (a) Sketch of experimental setup. ^{87}Rb atoms (green) are trapped in nine optical tweezers and coherently manipulated using microwave radiation (red ellipse). The direction of a magnetic bias field \vec{B}^{bias} (blue arrow) can be rotated in any direction given by Euler angles α and β defined in the laboratory frame $(\vec{x}, \vec{y}, \vec{z})$. The bias coils form a non-orthogonal coordinate frame $(\vec{x}_c, \vec{y}_c, \vec{z}_c)$ with angles $(\delta\beta_x, \delta\alpha_y, \delta\beta_y)$ relative to the laboratory frame. (b) Hyperfine transitions (red) between Zeeman-sublevels of ^{87}Rb . (c) [left panel] Strength of the \mathcal{B}_{σ_-} component of a microwave field for all directions (α, β) of \vec{B}^{bias} in the laboratory frame for an example polarization ellipse. [center and right panels] Differences in measured and predicted \mathcal{B}_{σ_-} for the sample values of $\delta\beta_x$ and $\delta\beta_y$ are indicated.

demonstration. In trapped atom experiments, developing knowledge of applied microwave polarization can be useful, *e.g.* for optimization of atomic Rabi rates or characterization of effective magnetic fields in complex trapping potentials [31–36]. In the context of atomic magnetometry, we envision our technique will be most relevant to hot-vapor cells, where one can measure magnetic fields with greater precision and versatility.

We begin by describing our specific experimental setup, although the procedures we describe apply generally. We use single ^{87}Rb atoms loaded with 50%-probability into a regular 3×3 array of $1.7 \mu\text{m}$ -spaced optical tweezers [Fig. 1(a)] [36]. We use four levels of ^{87}Rb : A ground-state $|g\rangle = |F=1, m_F=1\rangle$ and three excited hyperfine states $|e_+\rangle = |2, 2\rangle$, $|e_\pi\rangle = |2, 1\rangle$ and $|e_-\rangle = |2, 0\rangle$ states. During the experiment, we first initialize the atoms in $|g\rangle$ and then address the excited states using σ_\pm and π -polarized light components of a 6.834-GHz-microwave field ($\lambda \approx 44 \text{ mm}$) with magnitude $|\vec{\mathcal{B}}^{\mu\text{w}}|_{\text{max}} \equiv \|\vec{\mathcal{B}}^{\mu\text{w}}\| \approx 7.8 \mu\text{T}$ [Fig. 1(b)].

The transitions are split by a 300- μT -strong static

magnetic bias field \vec{B}^{bias} . The maximal splitting ($\sim 4.2 \text{ MHz}$) is $< 0.1\%$ of the microwave frequency, and hence spatial field differences are irrelevant when resonant with a transition. \vec{B}^{bias} is controlled by three coil pairs in near-Helmholtz configurations that define a coil-frame $\mathcal{C} = (\vec{x}_c, \vec{y}_c, \vec{z}_c)$ that importantly is not necessarily orthogonal. An orthonormal laboratory frame $\mathcal{L} = (\vec{x}, \vec{y}, \vec{z})$ is chosen s.t. \vec{z} [Euler angles: $(\alpha, \beta) = (0, 0)$] is oriented along \vec{z}_c , and \vec{x}_c and \vec{y}_c point in directions given by angles $(0, \pi/2 + \delta\beta_x)$, and $(\pi/2 + \delta\alpha_y, \pi/2 + \delta\beta_y)$, respectively [Fig. 1(a)].

We then determine the full polarization ellipse (*PE*) of the magnetic component of our microwave excitation field, expressed in \mathcal{L} as:

$$\vec{\mathcal{B}}^{\mu\text{w}} = \sum_{j \in \{x, y, z\}} \frac{1}{2} \mathcal{B}_j e^{-i(\phi_j + \omega t)} \vec{e}_j + \text{c.c.} \quad (1)$$

$\vec{\mathcal{B}}^{\mu\text{w}}$ traces the *PE* determined by 5 independent parameters: 3 fields $(\mathcal{B}_x, \mathcal{B}_y, \mathcal{B}_z)$ and two relative phases (ϕ_x, ϕ_y) , where $\phi_z = 0$ without loss of generality [37].

The quantization axis of our atoms, defined along \vec{B}^{bias} , is always well-defined because $\|\vec{\mathcal{B}}^{\mu\text{w}}\| \ll |\vec{B}^{\text{bias}}|$. The microwave field amplitudes $\mathcal{B}_{\pm\sigma}$ and \mathcal{B}_π that drive the $\Delta m_F = \pm 1$ and $\Delta m_F = 0$ atomic transitions, respectively, are strongly dependent on the direction of \vec{B}^{bias} and hence denoted as $\mathcal{B}_i^{(\alpha, \beta)}$ for $i \in (\sigma_\pm, \pi)$ hereafter. The $\mathcal{B}_i^{(\alpha, \beta)}$ are related to the 5 polarization-ellipse parameters and the direction of the bias field (α, β) by [37]:

$$\begin{aligned} (\mathcal{B}_\pi^{(\alpha, \beta)})^2 &= \mathcal{B}_z^2 \cos^2(\beta) \\ &+ (\mathcal{B}_x^2 \cos^2(\alpha) + \mathcal{B}_y^2 \sin^2(\alpha)) \sin^2(\beta) \\ &+ \mathcal{B}_z \mathcal{B}_x \sin(2\beta) \cos(\alpha) \cos(\phi_x) \\ &+ \mathcal{B}_z \mathcal{B}_y \sin(2\beta) \sin(\alpha) \cos(\phi_y) \\ &+ \mathcal{B}_y \mathcal{B}_x \sin(2\alpha) \sin^2(\beta) \cos(\phi_x - \phi_y) \end{aligned} \quad (2a)$$

$$\begin{aligned} (\mathcal{B}_{\pm\sigma}^{(\alpha, \beta)})^2 &= \frac{1}{2} \left(\sum_{j \in \{x, y, z\}} \mathcal{B}_j^2 - [\mathcal{B}_\pi^{(\alpha, \beta)}]^2 \right) \\ &\pm \mathcal{B}_x \mathcal{B}_y \cos(\beta) \sin(\phi_x - \phi_y) \\ &\mp \mathcal{B}_x \mathcal{B}_z \sin(\alpha) \sin(\beta) \sin(\phi_x) \\ &\pm \mathcal{B}_y \mathcal{B}_z \cos(\alpha) \sin(\beta) \sin(\phi_y). \end{aligned} \quad (2b)$$

Therefore, to recreate the full *PE*, 5 independent measurements of $(\mathcal{B}_{\pm\sigma}^{(\alpha, \beta)}, \mathcal{B}_\pi^{(\alpha, \beta)})$ can solve for the 5 unknown ellipse parameters [37]. For this, one can either vary (α, β) or the atomic transition.

In order to avoid systematic errors that may enter this procedure, we accurately extract $\mathcal{B}_i^{(\alpha, \beta)}$ from the corresponding (measured) Rabi frequency $\Omega_i^{(\alpha, \beta)} = \mu_i \mathcal{B}_i^{(\alpha, \beta)} / \hbar$. This, when referenced to a frequency stan-

dard, determines $\mathcal{B}_i^{(\alpha,\beta)}$ absolutely if the magnetic transition dipole moment μ_i is calculated from basic assumptions [38]. We measure $\Omega_i^{(\alpha,\beta)}$ using (pulsed) coherent population transfer [28, 30, 37–40], in which we apply a resonant microwave pulse of varying duration and fit the oscillating population in the atomic ground state [38].

However, systematic errors also enter through discrepancies of the intended and actual applied direction (α, β) of \vec{B}^{bias} . When performing any directional measurement with an atom(-like) system this is a general limitation which is typically addressed by referencing to an externally-calibrated system. Now let values $\{U_j\}$, $j \in [1, N^u]$ describe the N^u unknown systematic errors that modify the value and direction of \vec{B}^{bias} . The $\{U_j\}$ can be self-calibrated by performing $\geq N^u$ additional measurements and then solving the system of $\geq N^u + 5$ equations for $(\mathcal{B}_x, \mathcal{B}_y, \mathcal{B}_z, \phi_x, \phi_y; \{U_j\})$.

In our experiment, parameters $\{U_j\}$ are: orientations of the coil pairs $(U_1, U_2, U_3) = (\delta\beta_x, \delta\beta_y, \delta\alpha_y)$ forming \mathcal{C} [Fig. 1(a)], components of a (stray) magnetic field $(U_4, U_5, U_6) = (B_x^s, B_y^s, B_z^s)$ due to imperfect cancellation of ambient magnetic fields, and calibration errors $(U_7, U_8, U_9) = (|\vec{B}^{\text{bias}}|, \epsilon_x, \epsilon_y)$ in $\vec{B}^{\text{bias}} = |\vec{B}^{\text{bias}}|(\epsilon_x b_x, \epsilon_y b_y, b_z)$ using the parametrization $\sum_{i \in (x,y,z)} b_i^2 = 1$ [38]. Note, this set of parameters also includes the magnitude of \vec{B}^{bias} that will be determined from Zeeman shifts, which is irrelevant for determining a PE, but defines a common scaling factor for all static fields. We therefore need ≥ 14 measurements to self-calibrate our magnetometer and the bias-field strength.

Our self-calibration of the $\{U_j\}$ stems from the structure of the microwave light dictated by Maxwell's equations. To illustrate the key idea, we consider two simple examples where either $U_1 = \delta\beta_x$ or $U_2 = \delta\beta_y$ are unknown. Assume all of the N^u measurements are performed on the $\mathcal{B}_{\sigma_-}^{(\alpha,\beta)}$ -component of an elliptically polarized microwave field. The expected values of \mathcal{B}_{σ_-} for an example PE are shown in \mathcal{L} as a function of (α, β) [Fig. 1(c)]. If \mathcal{C} deviates from \mathcal{L} such that $(\beta_x, \beta_y) = (0, 0.05\pi)$, the functional form of $\mathcal{B}_{\sigma_-}^{(\alpha,\beta)} = \mathcal{B}_{\sigma_-}(\alpha, \beta; \beta_y)$ will deviate from the expectation in \mathcal{L} with a specific pattern $\Delta\mathcal{B}_{\sigma_-}$ [center panel in Fig. 1(c)]. This field pattern cannot be reproduced by allowed microwave ellipses, and is distinctly connected to the unknown parameter. Importantly, a different pattern is associated with $(\beta_x, \beta_y) = (0.05\pi, 0)$ [right panel in Fig. 1(c)]. Suitably chosen measurements can hence lead to full differentiation and absolute characterization of the unknowns $\{U_j\}$.

To calibrate the 9 $\{U_j\}$, we measure $\mathcal{B}_{\sigma_-}^{(\alpha,\beta)}$ (together with the Zeeman-shift of the σ_- -transition) for 28 different directions (α, β) [black points in Fig. 2(a)]. Using quadratic minimization [38] and Eq. (2b), these are enough measurements to determine $(\delta\beta_x, \delta\alpha_y, \delta\beta_y) = (1.3 \text{ mrad}, 10.9 \text{ mrad}, 5.4 \text{ mrad})$, $(B_x^s, B_y^s, B_z^s) =$

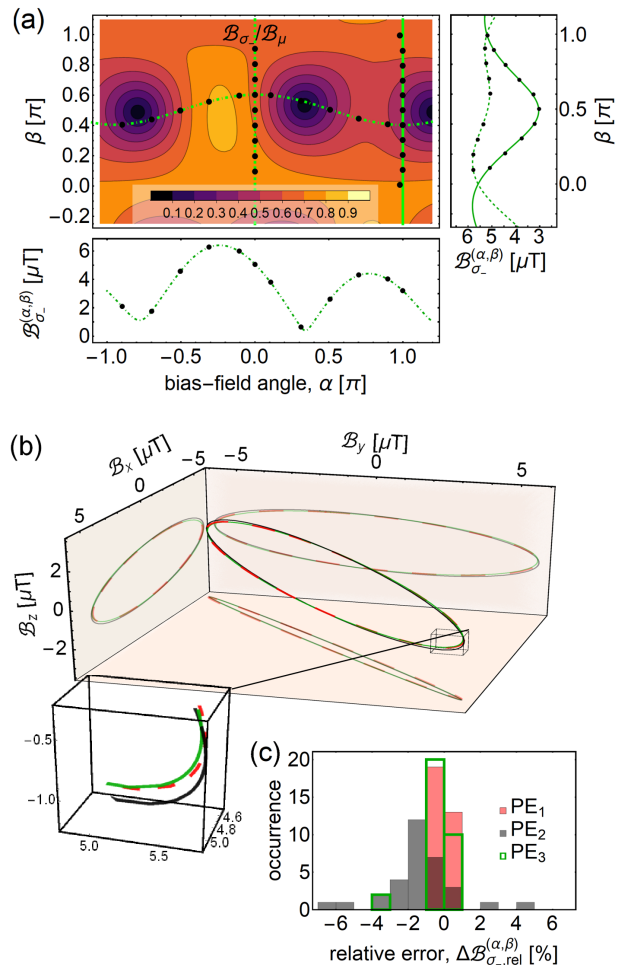


FIG. 2. (a) (2D-plot) Predicted magnetic field component $\mathcal{B}_{\sigma_-}^{(\alpha,\beta)}$ using parameters from the polarization ellipse PE_1 , as a function of the bias-field direction (α, β) . (small panels) Measured magnetic microwave field component (black data) and predictions along the solid, dashed, and dot-dashed cuts in the 2D-plot, respectively. The measurement uncertainties are smaller than the datapoints. (b) Polarization ellipses PE_1 (dashed, red), PE_2 (black) and PE_3 (green), respectively. PE_1 is the reference ellipse from the 28 calibration measurements of $\mathcal{B}_{\sigma_-}^{(\alpha,\beta)}$ from panel (a). Comparison of ellipses PE_2 (PE_3) assess our protocol using 5 of 6 measurements [38] without (with) taking into account calibrated $\{U_j\}$, see text. (c) Overlaid histograms of the relative errors $\Delta\mathcal{B}_{\sigma_-}^{(\alpha,\beta)}$ of all polarization ellipses and for all measurements displayed in panel (a). The colorcoding is the same as for panel (b).

$(-6.05 \mu\text{T}, 0.14 \mu\text{T}, -1.12 \mu\text{T})$, $|\vec{B}^{\text{bias}}| = 302.0 \mu\text{T}$, $(\epsilon_x, \epsilon_y) = (1.001, 0.989)$, and a polarization ellipse we refer to as PE_1 : $(\mathcal{B}_x, \mathcal{B}_y, \mathcal{B}_z, \phi_x, \phi_y) = (5.023(5) \mu\text{T}, 5.757(4) \mu\text{T}, 1.600(4) \mu\text{T}, -1.941(4), -1.873(4))$ [red, dashed ellipse in Fig. 2(b)]. We cannot extract uncertainties for the $\{U_j\}$, but estimations have shown that we need to vary a U_j by $\sim 20\%$ to change PE_1 by its uncertainty of $\lesssim 0.2\%$. Furthermore, the result is within expectation of experimentally-defined

parameters in our setup [38]; for example the angles measured are consistent with machining tolerances of the coil mounts. The measured Zeeman shift allows determination of $|\vec{B}^{\text{bias}}|$ which has a consistent dependence on (α, β) [38].

Figure 2(a) predicts $\mathcal{B}_{\sigma_-}^{(\alpha, \beta)}$ for all directions of \vec{B}^{bias} using Eq. (2b), and could be used to optimize atom-light coupling by choosing a suitable \vec{B}^{bias} . Furthermore, quantitative comparison with measurements indicates of how well $\{U_j\}$ and the ellipse parameters have been determined. For this, we investigate the relative errors $\Delta\mathcal{B}_{\sigma_-}^{(\alpha, \beta)}$ of all measured $\mathcal{B}_{\sigma_-}^{(\alpha, \beta)}$ and their predicted values [see red histogram Fig. 2(c)]. Not surprisingly, we find all $\Delta\mathcal{B}_{\sigma_-}^{(\alpha, \beta)}$ being distributed around 0, as they have been used to determine PE_1 . The width of the distribution is consistent with the $\mathcal{B}_{\sigma_-}^{(\alpha, \beta)}$ -measurement uncertainty of $\sim 0.1\%$, and a microwave-amplitude drift over several minutes of $\lesssim \pm 1\%$ [38]. This drift could be stabilized in future experiments.

We experimentally verify self-calibration by comparing polarization ellipses found using a completely independent set of measurements [black and green ellipses in Figure 2(b)]: $\mathcal{B}_{\sigma_+}^{(0,0)}$, $\mathcal{B}_{\sigma_-}^{(0,0)}$, $\mathcal{B}_{\sigma_+}^{(0, \pi/2 + \delta\beta_x)}$, $\mathcal{B}_{\pi}^{(0, \pi/2 + \delta\beta_x)}$, and $\mathcal{B}_{\sigma_-}^{(0, \pi/2 + \delta\beta_x)}$. Note, here we rotate our bias field from \vec{z}_c to \vec{x}_c in \mathcal{C} (only two directions!) and measure all three polarization components, in contrast to before, where we measured a single polarization for many directions. Still, using Eqs. (2), we determine the microwave field in all three dimensions.

The black ellipse (PE_2) is based on the wrong assumption that our coils are perfectly orthogonal, calibrated, and no stray magnetic fields are present ($U_j = 0$, except $U_7 = |\vec{B}^{\text{bias}}| = 300 \mu\text{T}$). The green ellipse (PE_3), takes into account the correctly calibrated $\{U_j\}$ and a microwave drift correction of 1% [38]. Both polarization ellipses PE_2 and PE_3 agree roughly with PE_1 in shape and size. However, PE_2 (wrong calibration) shows relative errors $\Delta\mathcal{B}_{\sigma_-}^{(\alpha, \beta)}$ larger than 5% which cannot be explained by microwave drifts or measurement uncertainties [Fig. 2(c)]. Contrary, PE_3 (using the correct $\{U_j\}$) predicts the (independent) 28 measurements correctly, *i.e.* the width of the $\Delta\mathcal{B}_{\sigma_-}^{(\alpha, \beta)}$ -distribution [Fig. 2(c)] is consistent with our microwave drifts [38].

With the microwave field as a static, well-calibrated reference in the laboratory frame \mathcal{L} , we now use the atoms to vectorially resolve a set of 3 intentionally applied static probe fields \vec{B}^{p} in \mathcal{L} . The procedure: combine any scalar atomic measurement of $|\vec{B}^{\text{p}}|$ with two Rabi-rate measurements to determine its orientation. Here, the $\sim 200 \mu\text{T}$ -strong-probe magnetic fields \vec{B}_j^{p} [$j = (x_c, y_c, z_c)$] are sequentially applied along \vec{x}_c , \vec{y}_c , and \vec{z}_c , respectively, in addition to a reference field $\{|\vec{B}^{\text{ref}}|, (\alpha, \beta)^{\text{ref}}\} \approx \{300 \mu\text{T}, (0.1\pi, 0.6\pi)\}$. We measure the total magnetic bias field $\vec{B}_j^{\text{m}} = \vec{B}_j^{\text{p}} + \vec{B}^{\text{ref}}$ (and for

completeness, \vec{B}^{ref}) and determine \vec{B}_j^{p} by subtraction of \vec{B}^{ref} . The use of a reference field $\vec{B}^{\text{ref}} \neq 0$ is not necessary, but can be useful [38]. All magnetic field *magnitudes* are found from the mean of the atomic Zeeman-shifts of all three available transitions. The *directions* $(\alpha, \beta)_j$ of \vec{B}_j^{m} and \vec{B}^{ref} are determined by measuring $\mathcal{B}_{\sigma_-}^{(\alpha, \beta)_j}$ and $\mathcal{B}_{\pi}^{(\alpha, \beta)_j}$ and then use Eq. (2) to solve for $(\alpha, \beta)_j$ via quadratic minimization [38]. We also measure $\mathcal{B}_{\sigma_+}^{(\alpha, \beta)_j}$, but use this for keeping track of drifts in the amplitude of our applied microwave field.

We find $\{|\vec{B}^{\text{ref}}|, (\alpha, \beta)^{\text{ref}}\} = \{296.6(2) \mu\text{T}, [0.103(1)\pi, 0.588(6)\pi]\}$ (brown lines). Sequential application of the 3 probe fields \vec{B}_j^{p} results in total measured fields $\{|\vec{B}_j^{\text{m}}|, (\alpha, \beta)_j^{\text{m}}\} = \{476.1(8) \mu\text{T}, [0.0636(6)\pi, 0.554(6)\pi]\}$, $\{301.5(3) \mu\text{T}, [0.108(2)\pi, 0.396(4)\pi]\}$, and $\{399.2(5) \mu\text{T}, [0.260(1)\pi, 0.577(2)\pi]\}$ [solid blue lines in Figure 3]. The multiple lines represent measurement uncertainties from bootstrapping the error with 200 trials. The difference in uncertainties for these measurements is determined by the precision with which we measure $\Omega_i^{(\alpha, \beta)}$, and by its transfer function to the field direction. This transfer function causes the uncertainties to be asymmetric (aspect ratios up to 30) and is linked to the choice of \vec{B}^{ref} [38].

We determine the mean probe fields $\vec{B}_j^{\text{p}} = \vec{B}_j^{\text{m}} - \vec{B}^{\text{ref}}$ (black) as the difference between the blue (\vec{B}_j^{m}) and the brown (\vec{B}^{ref}) vectors. The probe fields that we expect (red lines) point in \vec{x}_c , \vec{y}_c and \vec{z}_c -direction from \vec{B}^{ref} , and deviate from $\vec{B}_j^{\text{m}} - \vec{B}^{\text{ref}}$ by 16 mrad, 79 mrad and 23 mrad, respectively. For the \vec{y}_c and \vec{z}_c -direction, these values are just outside the confidence interval based

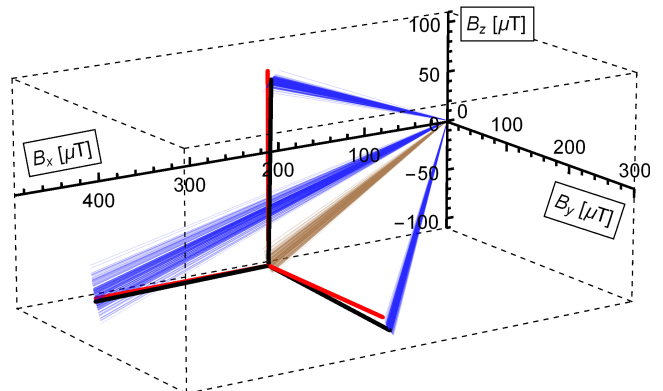


FIG. 3. Vector magnetometry in an orthonormal laboratory frame \mathcal{L} : Targeted (red) applied magnetic field vectors \vec{B}_j^{p} , $j \in (x_c, y_c, z_c)$, can be reconstructed (black) as the difference between all measured vectors \vec{B}_j^{m} (dark blue lines) and an initially applied reference field \vec{B}^{ref} (brown lines). The multiple lines for all displayed measured fields indicate the range of measurement errors, determined by bootstrapping the error with 200 trials.

on the measurement uncertainties, but can be fully explained when including the slow drift of the microwave field strength reported earlier [38]. Over the course of this set of measurements, this drift was found to be $\leq \pm 0.5\%$ as inferred from all the measured magnitudes $7.841(8) \mu\text{T}$, $7.840(6) \mu\text{T}$, $7.789(5) \mu\text{T}$, and $7.815(7) \mu\text{T}$, respectively.

The magnetometer can measure static and slowly varying magnetic fields, and can operate with (*reference*) or without \vec{B}^{ref} (*reference-free*, $|\vec{B}^{\text{p}}| \gg |\vec{B}^{\text{ref}}| \approx 0$). In *reference mode*, the uncertainty of \vec{B}^{ref} increases the uncertainty of \vec{B}_j^{p} , which is not the case for the *reference-free mode*. But $\vec{B}^{\text{ref}} \neq \vec{0}$ enables control over the magnetometers precision for a targeted parameter of interest and given noise sources, *e.g.* allowing "squeezing" the measured variance in certain directions [38]. Also, the *reference mode* avoids the complication of identifying the correct result out of 4 possible field solutions of Eqs. (2) [38], a challenge that can only be addressed in the *reference-free mode* with strategies such as an additional test-field [38].

Looking forward, we envision reconstruction of the microwave polarization ellipse to be a general-purpose reference for not only magnetic fields, but other excitation fields (*e.g.* optical fields or electric components). Further assessment is required to understand the potential for precision and sensitivity. Different measurement protocols should be developed to transition these ideas to scalable and more-sensitive atomic vapor cells. Coherent population transport was a robust way for us to measure microwave field strengths, but there are other ways to determine Rabi rates, *e.g.* by spectroscopic means. As with a variety of atomic sensors, this platform for vector magnetometry is compatible with futuristic quantum-enhancement, as established with cold atoms [41, 42].

ACKNOWLEDGMENTS

We thank M. Knill for his help with bootstrapping analysis. We thank Svenja Knappe, Philip Treutlein, Ronald Walsworth, Adam Kaufman for helpful discussions, and Chris Kiehl for technical assistance. T.T. acknowledges funding from SNF under project number: P2EZP2_172208. We acknowledge funding from NSF Grant No. PHYS 1734006, ONR Grant No. N00014-17-1-2245, AFOSR-MURI Grant No. FA9550-16-1-0323, and the David and Lucile Packard Foundation. M. O. B. acknowledges support from an NDSEG Fellowship.

* tobias.thiele@colorado.edu

† current address: CAS Key Laboratory of Microscale Magnetic Resonance and Department of Modern Physics,

University of Science and Technology of China, Hefei 230026, China; Synergetic Innovation Center of Quantum Information and Quantum Physics, University of Science and Technology of China, Hefei 230026, China

- [1] Arnold L. Bloom, "Principles of operation of the rubidium vapor magnetometer," *Appl. Opt.* **1**, 61–68 (1962).
- [2] Dmitry Budker and Michael Romalis, "Optical magnetometry," *Nature Physics* **3**, 227–234 (2007).
- [3] L. Rondin, J. P. Tetienne, T. Hingant, J. F. Roch, P. Maletinsky, and V Jacques, "Magnetometry with nitrogen-vacancy defects in diamond," *Reports on progress in physics* **77**, 056503 (2014).
- [4] Simon Gross, Christoph Barmet, Benjamin E. Dietrich, David O. Brunner, Thomas Schmid, and Klaas P. Pruessmann, "Dynamic nuclear magnetic resonance field sensing with part-per-trillion resolution," *Nature communications* **7**, 13702 (2016).
- [5] Reinhold Kleiner, Dieter Koelle, Frank Ludwig, and John Clarke, "Superconducting quantum interference devices: State of the art and applications," *Proceedings of the IEEE* **92**, 1534–1548 (2004).
- [6] Alexander F. H. Goetz, Barrett N. Rock, and Lawrence C. Rowan, "Remote sensing for exploration; an overview," *Economic Geology* **78**, 573–590 (1983).
- [7] A. B. Reid, J. M. Allsop, H. Granser, A. J. Millett, and I. W. Somerton, "Magnetic interpretation in three dimensions using euler deconvolution," *Geophysics* **55**, 80–91 (1990).
- [8] J. E. Lenz, "A review of magnetic sensors," *Proceedings of the IEEE* **78**, 973–989 (1990).
- [9] D. Budker and D. F. J. Kimball, *Optical Magnetometry* (Cambridge University Press, Oxford, 2013).
- [10] F. Camps, S. Harasse, and A. Monin, "Numerical calibration for 3-axis accelerometers and magnetometers," in *2009 IEEE International Conference on Electro/Information Technology* (2009) pp. 217–221.
- [11] Yan Xia Liu, Xi Sheng Li, Xiao Juan Zhang, and Yi Bo Feng, "Novel calibration algorithm for a three-axis strap-down magnetometer," *Sensors* **14**, 8485–8504 (2014).
- [12] Thiago P. Mayer Alegre, Charles Santori, Gilberto Medeiros-Ribeiro, and Raymond G. Beausoleil, "Polarization-selective excitation of nitrogen vacancy centers in diamond," *Phys. Rev. B* **76**, 165205 (2007).
- [13] B. J. Maertz, A. P. Wijnheijmer, G. D. Fuchs, M. E. Nowakowski, and D. D. Awschalom, "Vector magnetic field microscopy using nitrogen vacancy centers in diamond," *Appl. Phys. Lett.* **96**, 092504 (2010).
- [14] Pengfei Wang, Zhenheng Yuan, Pu Huang, Xing Rong, Mengqi Wang, Xiangkun Xu, Changkui Duan, Chenyong Ju, Fazhan Shi, and Jiangfeng Du, "High-resolution vector microwave magnetometry based on solid-state spins in diamond," *Nature communications* **6**, 6631 (2015).
- [15] Sang-Yun Lee, Matthias Niethammer, and Jörg Wrachtrup, "Vector magnetometry based on s=3/2 electronic spins," *Physical Review B* **92**, 115201 (2015).
- [16] Franz Münzhuber, Johannes Kleinlein, Tobias Kiessling, and Laurens W. Molenkamp, "Polarization-assisted vector magnetometry in zero bias field with an ensemble of nitrogen-vacancy centers in diamond," *arXiv preprint arXiv:1701.01089* (2017).
- [17] Jennifer M. Schloss, John F. Barry, Matthew J. Turner, and Ronald L. Walsworth, "Simultaneous broadband vector magnetometry using solid-state spins," *arXiv:1803.03718* (2018).

- [18] I. K. Kominis, T. W. Kornack, J. C. Allred, and M. V. Romalis, “A subfemtotesla multichannel atomic magnetometer,” *Nature* **422**, 596 (2003).
- [19] O. Gravrand, A. Khokhlov, Le Mouél J. L., and Léger J. M., “On the calibration of a vectorial ^4He pumped magnetometer,” *Earth, planets and space* **53**, 949–958 (2001).
- [20] A. K. Vershovskii, M. V. Balabas, A. É. Ivanov, V. N. Kulyasov, A. S. Pazgalev, and E. B. Aleksandrov, “Fast three-component magnetometer-variometer based on a cesium sensor,” *Technical Physics* **51**, 112–117 (2006).
- [21] S. J. Seltzer and M. V. Romalis, “Unshielded three-axis vector operation of a spin-exchange-relaxation-free atomic magnetometer,” *Applied physics letters* **85**, 4804–4806 (2004).
- [22] Antoine Weis, Georg Bison, and Anatoly S Pazgalev, “Theory of double resonance magnetometers based on atomic alignment,” *Physical Review A* **74**, 033401 (2006).
- [23] S. Pustelny, W. Gawlik, S. M. Rochester, D. F. Jackson Kimball, V. V. Yashchuk, and D. Budker, “Nonlinear magneto-optical rotation with modulated light in tilted magnetic fields,” *Phys. Rev. A* **74**, 063420 (2006).
- [24] Stuart J. Ingleby, Carolyn O’Dwyer, Paul F. Griffin, Aidan S. Arnold, and Erling Riis, “Vector magnetometry exploiting phase-geometry effects in a double-resonance alignment magnetometer,” arXiv preprint arXiv:1802.09273v1 (2018).
- [25] Kevin Cox, Valery I. Yudin, Alexey V. Taichenachev, Irina Novikova, and Eugeniy E. Mikhailov, “Measurements of the magnetic field vector using multiple electromagnetically induced transparency resonances in rb vapor,” *Phys. Rev. A* **83**, 015801 (2011).
- [26] Hwang Lee, Michael Fleischhauer, and Marlan O. Scully, “Sensitive detection of magnetic fields including their orientation with a magnetometer based on atomic phase coherence,” *Phys. Rev. A* **58**, 2587–2595 (1998).
- [27] B. Patton, E. Zhivun, D. C. Hovde, and D. Budker, “All-optical vector atomic magnetometer,” *Physical review letters* **113**, 013001 (2014).
- [28] C. Affolderbach, G. X. Du, T. Bandi, A. Horsley, P. Treutlein, and G. Miletì, “Imaging microwave and dc magnetic fields in a vapor-cell rb atomic clock,” *IEEE Transactions on Instrumentation and Measurement* **64**, 3629–3637 (2015).
- [29] Moto Kinoshita and Masanori Ishii, “Measurement of microwave magnetic field in free space using the rabi frequency,” in *Precision Electromagnetic Measurements (CPEM 2016), 2016 Conference on (IEEE, 2016)* pp. 1–2.
- [30] Andrew Horsley and Philipp Treutlein, “Frequency-tunable microwave field detection in an atomic vapor cell,” *Applied Physics Letters* **108**, 211102 (2016).
- [31] Fam Le Kien, Philipp Schneeweiss, and Arno Rauschenbeutel, “Dynamical polarizability of atoms in arbitrary light fields: general theory and application to cesium,” *Eur. Phys. J. D* **67**, 92 (2013).
- [32] J. D. Thompson, T. G. Tiecke, A. S. Zibrov, V. Vuletic, and M. D. Lukin, “Coherence and Raman sideband cooling of a single atom in an optical tweezer,” *Phys. Rev. Lett.* **110**, 133001 (2013).
- [33] Philipp Schneeweiss, Fam Le Kien, and Arno Rauschenbeutel, “Nanofiber-based atom trap created by combining fictitious and real magnetic fields,” *New Journal of Physics* **16**, 013014 (2014).
- [34] Jan Petersen, Jürgen Volz, and Arno Rauschenbeutel, “Chiral nanophotonic waveguide interface based on spin-orbit interaction of light,” *Science* **346**, 67–71 (2014).
- [35] A. Goban, C.-L. Hung, S.-P. Yu, J.D. Hood, J.A. Muniz, J.H. Lee, M.J. Martin, A.C. McClung, K.S. Choi, D.E. Chang, O. Painter, and H. J. Kimble, “Atom-Light Interactions in Photonic Crystals,” *Nat. Commun.* **5**, 3808 (2014).
- [36] A. M. Kaufman, *Laser-cooling atoms to indistinguishability: Atomic Hong-Ou-Mandel interference and entanglement through spin exchange*, Ph.D. thesis, University of Colorado at Boulder (2015).
- [37] J. Köpsell, T. Thiele, J. Deiglmayr, A. Wallraff, and F. Merkt, “Measuring the polarization of electromagnetic fields using rabi-rate measurements with spatial resolution: experiment and theory,” *Phys. Rev. A* **95**, 053860 (2017).
- [38] see supplementary information which includes references [43–50].
- [39] H. Q. Fan, S. Kumar, R. Daschner, H. Kübler, and J. P. Shaffer, “Sub-wavelength microwave electric-field imaging using Rydberg atoms inside atomic vapor cells,” *Opt. Lett.* **39**, 3030 (2017).
- [40] T. Thiele, J. Deiglmayr, M. Stammeier, J.-A. Agner, H. Schmutz, F. Merkt, and A. Wallraff, “Imaging electric fields in the vicinity of cryogenic surfaces using rydberg atoms,” *Phys.Rev. A* **92**, 063425 (2015).
- [41] W. Muessel, H. Strobel, D. Linnemann, D. B. Hume, and M. K. Oberthaler, “Scalable spin squeezing for quantum-enhanced magnetometry with bose-einstein condensates,” *Phys. Rev. Lett.* **113**, 103004 (2014).
- [42] C. L. Degen, F. Reinhard, and P. Cappellaro, “Quantum sensing,” *Rev. Mod. Phys.* **89**, 035002 (2017)
- [43] A. M. Kaufman, B. J. Lester, and C. A. Regal, “Cooling a Single Atom in an Optical Tweezer to Its Quantum Ground State,” *Phys. Rev. X* **2**, 041014 (2012).
- [44] Chung-Yu Shih and Michael S. Chapman, “Nondestructive light-shift measurements of single atoms in optical dipole traps,” *Phys. Rev. A* **87**, 063408 (2013).
- [45] Daniel A. Steck, *Rubidium 87 D Line Data*, published: available online at <http://steck.us/alkalidata> (revision 2.1.4, 23 December 2010).
- [46] D. Budker, D. F. Kimball, S. M. Rochester, V. V. Yashchuk, and M. Zolotarev, “Sensitive magnetometry based on nonlinear magneto-optical rotation,” *Physical Review A* **62**, 043403 (2000).
- [47] J. C. Allred, R. N. Lyman, T. W. Kornack, and M. V. Romalis, “High-sensitivity atomic magnetometer unaffected by spin-exchange relaxation,” *Physical review letters* **89**, 130801 (2002).
- [48] Andrew Horsley, Guan-Xiang Du, and Philipp Treutlein, “Widefield microwave imaging in alkali vapor cells with sub-100 um resolution,” *New Journal of Physics* **17**, 112002 (2015).
- [49] S. Afach, G. Ban, G. Bison, K. Bodek, Z. Chowdhuri, Z. D. Grujić, L. Hayen, V. Hélaine, M. Kasprzak, K. Kirch, P. Knowles, H.-C. Koch, S. Komposch, A. Kozela, J. Krempel, B. Lauss, T. Lefort, Y. Lemièrre, A. Mtchedlishvili, O. Naviliat-Cuncic, F. M. Piegsa, P. N. Prashanth, G. Quémener, M. Rawlik, D. Ries, S. Rocca, D. Rozpedzik, P. Schmidt-Wellenburg, N. Severjins, A. Weis, E. Wursten, G. Wyszynski, J. Zejma, and G. Zsigmond, “Highly stable atomic vector magnetometer based on free spin precession,” *Opt. Express* **23**, 22108–

- 22115 (2015).
- [50] Miroslav Gajdacz, Poul L. Pedersen, Troels Mørch, Andrew J. Hilliard, Jan Arlt, and Jacob F. Sherson, “Non-destructive faraday imaging of dynamically controlled ultracold atoms,” *Review of Scientific Instruments* **84**, 083105 (2013), <https://doi.org/10.1063/1.4818913>